

Continuous condensation in nanogrooves

Alexandr Malijevský

Department of Physical Chemistry, University of Chemical Technology Prague, Praha 6, 166 28, Czech Republic;
Department of Microscopic and Mesoscopic Modelling,
ICPF of the Czech Academy of Sciences, 165 02 Prague 6, Czech Republic

We consider condensation in a capillary groove of width L and depth D , formed by walls that are completely wet (contact angle $\theta = 0$), which is in a contact with a gas reservoir of the chemical potential μ . On a mesoscopic level, the condensation process can be described in terms of the midpoint height ℓ of a meniscus formed at the liquid-gas interface. For macroscopically deep grooves ($D \rightarrow \infty$), and in the presence of long-range (dispersion) forces, the condensation corresponds to a second order phase transition, such that $\ell \sim (\mu_{cc} - \mu)^{-1/4}$ as $\mu \rightarrow \mu_{cc}^-$ where μ_{cc} is the chemical potential pertinent to capillary condensation in a slit pore of width L . For finite values of D , the transition becomes rounded and the groove becomes filled with liquid at a chemical potential higher than μ_{cc} with a difference of the order of D^{-3} . For sufficiently deep grooves, the meniscus growth initially follows the power-law $\ell \sim (\mu_{cc} - \mu)^{-1/4}$ but this behaviour eventually crosses over to $\ell \sim D - (\mu - \mu_{cc})^{-1/3}$ above μ_{cc} , with a gap between the two regimes shown to be $\delta\mu \sim D^{-3}$. Right at $\mu = \mu_{cc}$, when the groove is only partially filled with liquid, the height of the meniscus scales as $\ell^* \sim (D^3 L)^{1/4}$. Moreover, the chemical potential (or pressure) at which the groove is half-filled with liquid exhibits a non-monotonic dependence on D with a maximum at $D \approx 3L/2$ and coincides with μ_{cc} when $L \approx D$. Finally, we show that condensation in finite grooves can be mapped on the condensation in capillary slits formed by two asymmetric (competing) walls a distance D apart with potential strengths depending on L . All these predictions, based on mesoscopic arguments, are confirmed by fully microscopic Rosenfeld's density functional theory with a reasonable agreement down to surprisingly small values of both L and D .

I. INTRODUCTION

Capillary condensation, i.e. the phenomenon whereby an undersaturated gas confined by solid walls condenses to a high density, liquidlike phase, is perhaps the most fundamental manifestation of surface tension and finite-size effects [1, 2]. For sufficiently wide pores, the difference in the chemical potential μ_{cc} at which the fluid condenses in an open slit pore formed of two parallel plates from the saturated chemical potential μ_{sat} is provided by the classical Kelvin equation which can be derived by combining the geometric properties of the pore with the properties of a meniscus formed at the gas-liquid interface. According to this macroscopic viewpoint, the meniscus is of a circular cross-section with a Laplace radius and meets both walls at Young's contact angle θ . However, the Kelvin equation becomes increasingly less reliable as the pore width L is decreased towards a molecular scale, especially when the side walls are completely wet $\theta = 0$. In this case, the slit walls are covered by liquidlike layers of width ℓ_π , so that the space between the walls available for the gas molecules is effectively reduced. The importance of the presence of the wetting layers on the location of capillary condensation was firstly recognized by Derjaguin's school using the concept of disjoining pressure [3] which has been later put into a more general picture of interfacial phenomena by Evans *et al.* [4, 5] within the framework of density functional theory [6]. It follows that the location of the capillary condensation phase transition in a slit exerting van der Waals (dispersion) forces is given by the modified Kelvin

equation

$$\mu_{cc}(L) = \mu_{\text{sat}} - \frac{2\gamma}{\Delta\rho(L - 3\ell_\pi)} \quad (1)$$

where γ is the gas-liquid surface tension and $\Delta\rho = \rho_l - \rho_g$ is the difference between the particle densities of the coexisting bulk phases. Note that the presence of the factor 3 in the denominator does not reflect the geometric restriction of the volume available to the gas molecules but rather the nature of the asymptotic behavior of the wall-fluid interaction.

More recently, fluid condensation in a much more experimentally realistic model of capillary grooves etched into a solid surface has attracted substantial attention [7–21]. Within this model, one considers an infinitely long slit of width L and depth D which is in contact with the bulk gas via the open top. For macroscopically deep grooves $D \rightarrow \infty$, the recent theoretical and experimental studies revealed that the nature of condensation in grooves differs considerably from that in open slits. Perhaps most importantly, the transition remains first-order only when the contact angle of the groove wall is finite $\theta > 0$. However, above the wetting temperature T_w when the walls are completely wet by liquid, i.e. $\theta = 0$, the condensation turns to be continuous (critical). In this case, the wetting layers at the side and bottom walls merge to form a meniscus, the mid-height ℓ of which increases continuously as μ_{cc} is approached from below and eventually diverges according to the power-law:

$$\ell \sim \delta\mu^{-\beta_C}, \quad (2)$$

as $\delta\mu \equiv \mu_{cc} - \mu \rightarrow 0^+$. The critical exponent β_C depends on the asymptotic behaviour of the microscopic

interactions and for van der Waals forces $\beta_C = 1/4$.

In this work, we consider *microscopically* deep grooves formed of walls interacting with the fluid via long range dispersion forces and we ask what the repercussions of finiteness of D are on the fluid condensation. As has been shown recently [22], the condensation remains continuous, although not critical since ℓ can not diverge anymore, so that the process does not exhibit any singular behaviour. However, we will show that condensation in finitely deep grooves in the presence of long-range forces experiences some new aspects, not present in the case of macroscopically deep grooves, as a consequence of the competition between effective repulsions from the groove top and groove bottom acting on the meniscus. To this end, we will compare analytic predictions based on a mesoscopic slab model with a microscopic fundamental measure density functional theory (DFT) which takes the packing effects, that for the highly geometrically restricted systems are of crucial importance, accurately into account and obeys the statistical mechanical sum rules, as opposed to some less sophisticated DFT versions.

In the remainder of this paper we will first formulate the microscopic model based on DFT and determine the external field exerted by the groove walls (section II). In section III we revisit the slab model used previously to study the criticality of condensation in infinitely deep grooves [13] which we extend for finite D and compare with the results obtained numerically from DFT. We conclude by summarizing and discussing the main results in section IV and show some details of our calculations based on the slab model in Appendix A.

II. MICROSCOPIC MODEL

In the classical density functional theory [6], the equilibrium density profile minimises the grand potential functional

$$\Omega[\rho] = \mathcal{F}[\rho] + \int d\mathbf{r} \rho(\mathbf{r}) [V(\mathbf{r}) - \mu], \quad (3)$$

where μ is the chemical potential, and $V(\mathbf{r})$ is the external potential. The intrinsic free energy functional $\mathcal{F}[\rho]$ can be separated into an exact ideal gas contribution and an excess part:

$$\mathcal{F}[\rho] = \beta^{-1} \int d\mathbf{r} \rho(\mathbf{r}) [\ln(\rho(\mathbf{r})\Lambda^3) - 1] + \mathcal{F}_{\text{ex}}[\rho], \quad (4)$$

where Λ is the thermal de Broglie wavelength and $\beta = 1/k_B T$ is the inverse temperature. As is common in the modern DFT approaches, the excess part is modelled as a sum of hard-sphere and attractive contributions where the latter is treated in a simple mean-field fashion:

$$\mathcal{F}_{\text{ex}}[\rho] = \mathcal{F}_{\text{hs}}[\rho] + \frac{1}{2} \int \int d\mathbf{r} d\mathbf{r}' \rho(\mathbf{r}) \rho(\mathbf{r}') u_{\text{a}}(|\mathbf{r} - \mathbf{r}'|), \quad (5)$$

where $u_{\text{a}}(r)$ is the attractive part of the fluid-fluid interaction potential.

The fluid atoms are assumed to interact with one another via the truncated (i.e., short-ranged) and non-shifted Lennard-Jones-like potential

$$u_{\text{a}}(r) = \begin{cases} 0; & r < \sigma, \\ -4\varepsilon \left(\frac{\sigma}{r}\right)^6; & \sigma < r < r_c, \\ 0; & r > r_c. \end{cases} \quad (6)$$

which is cut-off at $r_c = 2.5\sigma$, where σ is the hard-sphere diameter.

The hard-sphere part of the excess free energy is approximated using the (original) Rosenfeld fundamental measure functional [23],

$$\mathcal{F}_{\text{hs}}[\rho] = \frac{1}{\beta} \int d\mathbf{r} \Phi(\{n_{\alpha}\}), \quad (7)$$

which accurately takes into account the short-range correlations between the fluid particles.

We assume that the confining walls are formed by atoms distributed uniformly with a density ρ_w and interact with the fluid particles via Lennard-Jones 12-6 potential $\phi_w(r)$ with the parameters ε_w and σ :

$$\phi_w(r) = 4\varepsilon_w \left[\left(\frac{\sigma}{r}\right)^{12} - \left(\frac{\sigma}{r}\right)^6 \right]. \quad (8)$$

The wall potential containing a single groove of depth D and width L , which is located at $0 < x < L$ and $0 < z < D$, can be expressed as follows:

$$V(x, z) = V_{9-3}(z) + V_D(x, z) + V_D(L - x, z), \quad (9)$$

except for the region corresponding to the domain of the wall in which case $V(x, z) = \infty$ meaning the wall is impenetrable. We assume that the groove is macroscopically long and the system is thus translation invariant along the y -axis. Here, $V_{9-3}(z)$ is the well known 9-3 Lennard-Jones potential due to a planar wall placed at $z < 0$:

$$V_{9-3}(z) = 4\pi\varepsilon_w\rho_w\sigma^3 \left[\frac{1}{45} \left(\frac{\sigma}{z}\right)^9 - \frac{1}{6} \left(\frac{\sigma}{z}\right)^3 \right]. \quad (10)$$

The potential $V_D(x, z)$, corresponding to a semi-infinite slab of height D placed at $x < 0$ and $0 < z < D$, is determined by evaluating the triple integral:

$$\begin{aligned} V_D(x, z) &= \rho_w \int_{-\infty}^0 dx' \int_{-\infty}^{\infty} dy' \int_0^D dz' \\ &\quad \times \phi_w \left(\sqrt{(x-x')^2 + y'^2 + (z-z')^2} \right) \\ &= \alpha_6 [\psi_6(x, z) + \psi_6(x, D-z)] \\ &\quad + \alpha_{12} [\psi_{12}(x, z) + \psi_{12}(x, D-z)] \end{aligned} \quad (11)$$

where

$$\psi_6(x, z) = \frac{2x^4 + x^2z^2 + 2z^4}{2x^3z^3\sqrt{x^2 + z^2}} - \frac{1}{z^3} \quad (12)$$

and

$$\psi_{12}(x, z) = \frac{1}{128} \frac{128x^{16} + 448x^{14}z^2 + 560x^{12}z^4 + 280x^{10}z^6 + 35x^8z^8 + 280x^6z^{10} + 560x^4z^{12} + 448z^{14}x^2 + 128z^{16}}{z^9x^9(x^2+z^2)^{7/2}} - \frac{1}{z^9} \quad (13)$$

with $\alpha_6 = -\pi\varepsilon_w\rho_w\sigma^6/3$ and $\alpha_{12} = 2\pi\varepsilon_w\rho_w\sigma^{12}/45$.

Minimization of (3) leads to the Euler-Lagrange equation

$$V(\mathbf{r}) + \frac{\delta\mathcal{F}_{\text{hs}}[\rho]}{\delta\rho(\mathbf{r})} + \int d\mathbf{r}'\rho(\mathbf{r}')u_a(|\mathbf{r}-\mathbf{r}'|) = \mu, \quad (14)$$

which can be solved iteratively on an appropriately discretized two dimensional grid $(0, x_m) \times (0, z_m)$. The system size is determined by the values $x_m > L$ and $z_m > D$ that are chosen large enough to justify the following boundary conditions that we impose: $\rho(x, z_m) = \rho_b$ and $\rho(0, z) = \rho(x_m, z) = \rho_\pi(z)$ for $z > D$ where ρ_b is the reservoir gas density and $\rho_\pi(z)$ is a 1D density profile of the model fluid near a planar wall.

Prior applying our microscopic model to study condensation in capillary grooves, we investigate the bulk phase behaviour of the model fluid by setting $V(\mathbf{r}) = 0$ in Eq. (14); in particular we obtain that the bulk critical temperature corresponds to $k_B T_c/\varepsilon = 1.414$. Furthermore, by setting $V(\mathbf{r}) = V_{9-3}(z)$ with a parameter $\rho_w\varepsilon_w = 1 \cdot \varepsilon\sigma^{-3}$ we find that the wall-fluid system exhibits a first-order wetting phase transition at temperature $T_w = 0.8T_c$. Finally, a slit model formed by a pair of parallel walls with the total potential $V(\mathbf{r}) = V_{9-3}(z) + V_{9-3}(L-z)$ for the slit width $L = 20\sigma$ and temperature $T = 1.15T_w$ (to be considered later for the groove models) experiences capillary condensation at the chemical potential $\mu_{cc} = -4.018\varepsilon$. We note that although the external potentials and thus the resulting equilibrium density profiles vary only in one dimension in these systems, we treat them in the same way as the groove model, i.e. we determine $\rho(\mathbf{r}) = \rho(x, z)$ for the sake of numerical consistency.

III. RESULTS

In this section we present the DFT results of the condensation in grooves of finite depth D and width L formed of completely wet walls and compare with predictions based on a slab model [24]. The slab model has been used previously [13, 18] to analyze the critical behaviour of condensation and evaporation in infinitely deep grooves and it is straightforward to extend the analysis for grooves of finite depths. Within the model one assumes that the one-body fluid density $\rho(\mathbf{r}) = \rho(x, z)$ adopts only three values: i) $\rho(\mathbf{r}) = \rho_l$, the liquid density at bulk two-phase coexistence, if the fluid occupies the volume near the side and bottom walls as described in Fig. 1; here, the meniscus is approximated by a flat interface of height ℓ above the groove bottom, while the

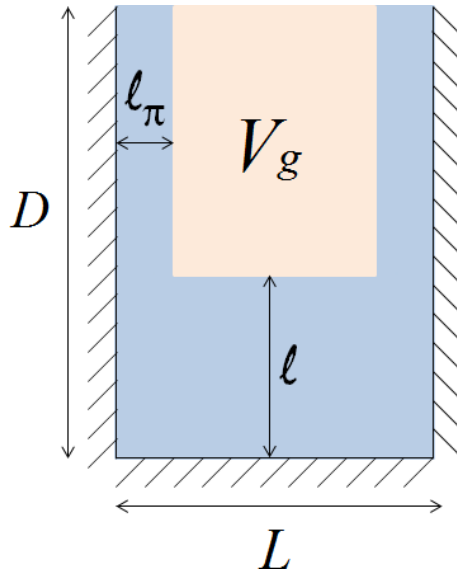


FIG. 1: Illustration of the slab model applied for a groove of depth D and width L . The adsorbing wetting layers are of the width ℓ_π and the height of the “meniscus” is ℓ . The remaining volume V_g is occupied by a gas-like phase.

width of the wetting layers at each of the side walls is ℓ_π ; ii) $\rho(\mathbf{r}) = \rho_g$, the vapour density at bulk two-phase coexistence, if the fluid occupies the region of the cross-section area $V_g = (L - 2\ell_\pi)(D - \ell)$; and (iii) $\rho(\mathbf{r}) = 0$ otherwise, since the groove walls are impenetrable. As in our microscopic model described in the previous section we consider grooves that are macroscopically long, so that we assume that the system is translation invariant along the y -axis normal to the sketch of Fig. 1.

The groove is in contact with a gas reservoir of pressure p , so that the adsorbed liquid phase which is metastable in bulk must have a lower pressure p^\dagger . For this model, the excess (relative to the groove completely filled with liquid) grand potential per unit length is given by

$$\begin{aligned} \omega^{\text{ex}}(\tilde{\ell}) &= (p^\dagger - p)(L - 2\ell_\pi)(D - \tilde{\ell}) \\ &+ \gamma[2(D - \tilde{\ell}) + (L - 2\ell_\pi)] \\ &- \Delta\rho \int_{\tilde{\ell}}^D dz \int_{\ell_\pi}^{L-\ell_\pi} dx V(x, z) \quad (15) \end{aligned}$$

where $V(\mathbf{r}) = V(x, z)$ is the external potential of the groove walls as given by Eq. (9). Approximating the pressure difference $p - p^\dagger \approx \Delta\rho(\mu_{\text{sat}} - \mu)$, obtained by Taylor expansion of $p(\mu)$ around μ_{sat} to first order, the equilibrium mean height of the liquid slab ℓ is determined

by minimizing $\omega^{\text{ex}}(\tilde{\ell})$ which leads to

$$\mu(\ell) \approx \mu_{cc}(L) + a \left[\frac{2}{(D-\ell)^3} - \frac{9L}{8\ell^4} \right]. \quad (16)$$

Here, we made use of Eq. (1) and introduced $a = \pi\varepsilon_w\rho_w\sigma^6/3$ related to the Hamaker constant. The corresponding thermodynamic excess grand potential can be expressed in the form of the series:

$$\begin{aligned} \frac{\omega^{\text{ex}}}{(L-2\ell_\pi)} &= \delta\mu\Delta\rho\ell + \frac{\pi L\varepsilon_w}{8\ell^3} + \dots \\ &+ \frac{\pi\varepsilon_w}{3(D-\ell)^2} + \dots \end{aligned} \quad (17)$$

where the ellipses denote the higher order terms in $1/\ell$ and $1/(D-\ell)$ and where we ignored irrelevant terms not dependent on ℓ . In deriving Eq. (16), all the contributions beyond the leading order terms in $1/\ell$ and $1/(D-\ell)$ have been neglected which suggests that (16) is only reliable for i) sufficiently deep grooves and ii) near μ_{cc} ; it is only in this case when both ℓ and $D-\ell$ are supposed to be large (compared, e.g., to σ).

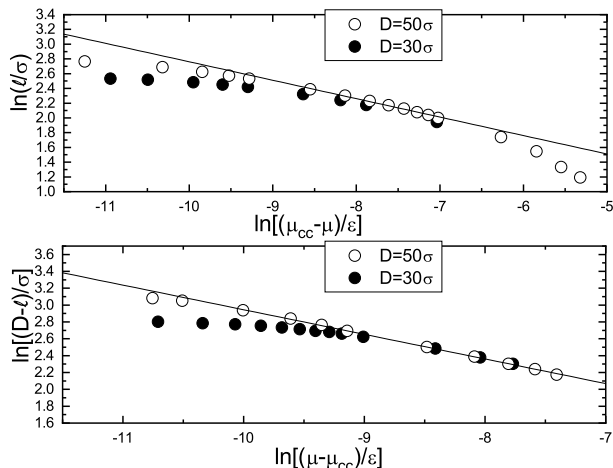


FIG. 2: A log-log plot for condensation in grooves of depth $D = 30\sigma$ and $D = 50\sigma$, each of width $L = 20\sigma$, above the wetting temperature $T = 1.15T_w$. The upper panel describes the regime $\mu < \mu_{cc}$ and the straight line has a slope $-1/4$, while the lower panel describes the regime $\mu > \mu_{cc}$ and the straight line has a slope $-1/3$.

For infinitely (macroscopically) deep grooves, $D \rightarrow \infty$, Eq. (16) immediately reproduces the value of the critical exponent $\beta_C = 1/4$, corresponding to a divergence of ℓ as $\mu \rightarrow \mu_{cc}^-$; in this case the terms $\mathcal{O}((D-\ell)^{-3})$ can be neglected. Moreover, it also implies a divergence of $D-\ell$ as μ_{cc} is approached from above pertinent to evaporation of capillary liquid, characterized by a critical exponent $\beta_E = 1/3$, in which case the terms $\mathcal{O}(\ell^{-4})$ can be neglected. For grooves of finite depths both $\mathcal{O}((D-\ell)^{-3})$ and $\mathcal{O}(\ell^{-4})$ are relevant and represent competing repulsions from the groove bottom and groove top acting effectively on the meniscus of height ℓ . Hence, condensation in grooves of finite depths undergoes two regimes:

$\mu < \mu_{cc}$ in which case the term L/ℓ^4 in Eq. (16) representing repulsion from the groove bottom is dominating and $\mu > \mu_{cc}$ in which case the repulsion from the groove top $\propto 1/(D-\ell)^3$ prevails. The repulsion from the groove top implies that grooves of finite depths become largely filled with liquid at a chemical potential μ_f which is higher than μ_{cc} as for infinitely deep grooves. Introducing a small parameter α by defining a meniscus height of a filled groove $\ell = (1-\alpha)D$ where $\alpha \ll 1$ and substituting to Eq. (16), we find that $\mu_f \approx \mu_{cc} + 2a/(\alpha D)^3$.

The impact of the finite depth of grooves has been inspected by considering two systems with $D = 50\sigma$ and $D = 30\sigma$, both of width $L = 20\sigma$, at temperature $T = 1.15T_w$. The DFT results are displayed in Fig. 2 where we show the dependence of $\ell(\mu)$ below and above μ_{cc} as a log-log plot. We observe a crossover from the $\ell \propto \delta\mu^{-1/4}$ behaviour to the $D-\ell \propto |\delta\mu|^{-1/3}$ dependence, such that the two regimes are separated by a gap of the order of $\bar{\delta}\mu$. In Appendix A we show that

$$\bar{\delta}\mu = \frac{a}{D^3}, \quad (18)$$

as follows from our slab model. This result can be quantitatively verified by substituting the values corresponding to the DFT model at the considered temperature, which yields $a \approx 0.3$. It then follows that $\ln(\bar{\delta}\mu) \approx -9$ for $D = 30\sigma$ and $\ln(\bar{\delta}\mu) \approx -10.5$ for $D = 50\sigma$, with a fairly good agreement with the DFT results.

Some more details of the fluid behaviour inside our capillary groove model can be revealed by determining two-dimensional density profiles as shown in Fig. 3 for several illustrative chemical potentials. We observe that in line with our expectations a well pronounced meniscus forms at the liquid-gas interface despite strong packing effects near the walls that make the fluid distribution strongly inhomogeneous. The meniscus indeed shifts continuously upwards as the chemical potential increases from $\mu < \mu_{cc}$ to $\mu > \mu_{cc}$ and also note that thin wetting layers form at the side walls as consistent with our slab model, unless the meniscus is located near the groove top.

Since grooves of finite D are only partially filled with liquid at $\mu = \mu_{cc}$, one may enquire what the dependence of the meniscus height $\ell^* = \ell(\mu_{cc})$ is on the groove parameters. This height characterizes a location at which the condensation regime changes from $\ell \approx \delta\mu^{-1/4}$ to $\ell \approx D - |\delta\mu|^{-1/3}$ and when the effective repulsive forces just balance. From the slab model it follows directly that

$$\frac{\ell^*}{L} \sim \left(\frac{D}{L} \right)^{\frac{3}{4}}, \quad (19)$$

for sufficiently large D . We test this result by comparing with the microscopic DFT model as is shown in Fig. 4 as a log-log plot; we observe that the scaling form of Eq. (19) is obeyed accurately even down to very small values of D of the order of just units of molecular diameters. This is surprising, since one would expect any mesoscopic predictions to break down when $D < L/2$ not allowing for

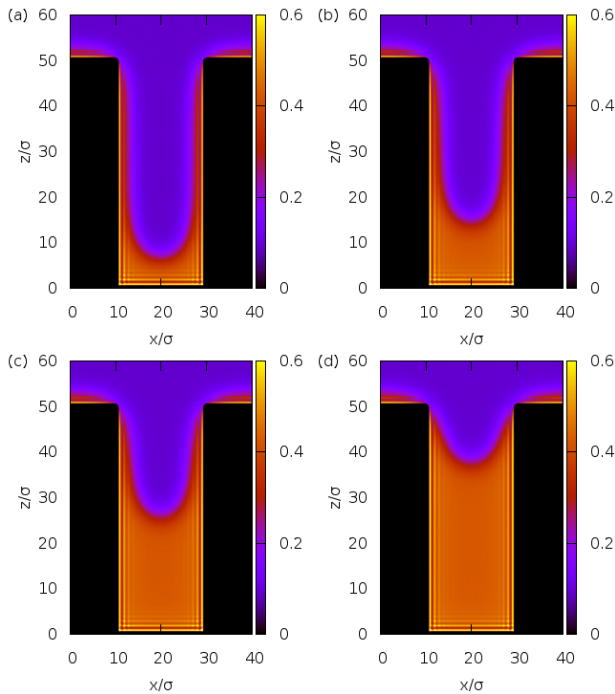


FIG. 3: Two-dimensional DFT equilibrium density profiles corresponding to condensation in the capillary groove of depth $D = 50\sigma$ and width $L = 20\sigma$, at temperature $T = 1.15T_w$. The departure $\delta\mu = \mu_{cc} - \mu$ from the chemical potential pertinent to capillary condensation in an infinite slit of the same width is (in units of ε): a) 0.07, b) 0, c) -0.001, and d) -0.004.

a meniscus formation. It suggests that the nature of the condensation is governed by the presence of the long-range microscopic interactions (precisely included in our slab model) rather than by a meniscus shape which was approximated rather crudely.

The previous result, namely the non-linear dependence of $\ell(D)$, is a consequence of the asymmetry in the range of the two effective repulsions. Another implication of this, also absent for infinitely deep grooves, can be addressed by determining the dependence of the chemical potential $\mu_{\frac{1}{2}}$ at which the groove is half-filled with liquid on groove depth D . This is obtained by substituting for $\ell = D/2$ into Eq. (16) which yields

$$\mu_{\frac{1}{2}} = \mu_{cc} + 2a \left(\frac{8}{D^3} - \frac{9L}{D^4} \right). \quad (20)$$

From here it follows that $\mu_{\frac{1}{2}}(D)$ asymptotically approaches μ_{cc} from above as $1/D^3$. However, the function reaches its maximum at $D = 3L/2$ below which the last term in (20) becomes dominating and $\mu_{\frac{1}{2}}$ decreases rapidly with decreasing D . This also implies that there exists a unique finite value D^* (for the given L and T) for which the groove is half filled exactly at μ_{cc} . These predictions have been tested against the DFT model and the comparison is displayed in Fig. 5. There is a good overall agreement between the two theories although the

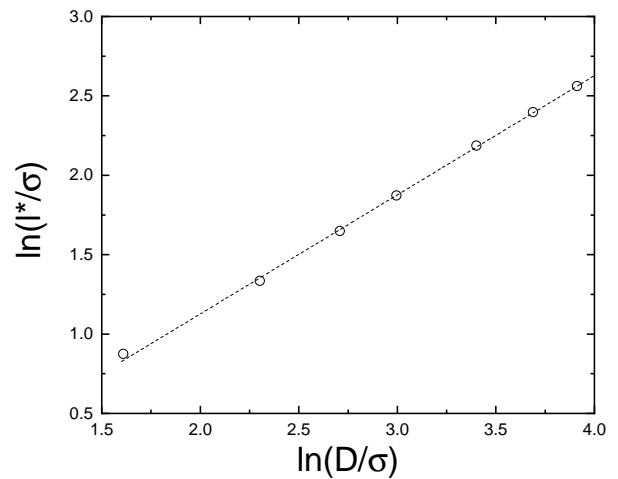


FIG. 4: A log-log plot of the dependence of the meniscus height $\ell^* = \ell(\mu_{cc})$ on groove depth D as obtained from DFT (symbols). The dashed line is the fit $y = y_0 + 0.75x$, a dependence corresponding to the slab model as given by Eq. (19), to the DFT data.

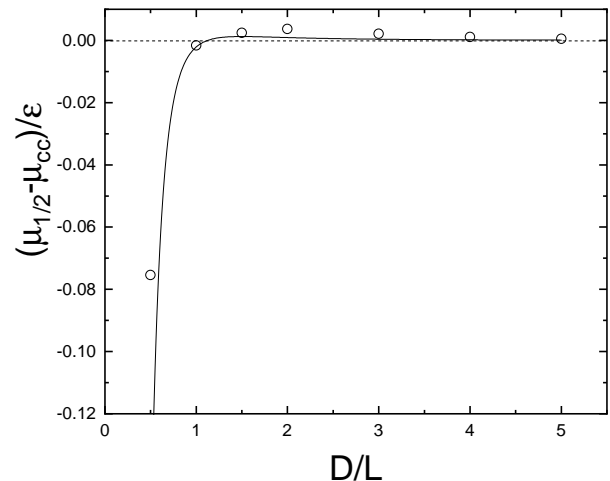


FIG. 5: Dependence of the chemical potential $\mu_{\frac{1}{2}}$ at which the groove is half-filled with liquid, i.e. $\ell = D/2$, on the groove depth D . The symbols denote DFT results and the solid line denotes the prediction of the slab model, Eq. (16).

location of the maximum of $\mu_{\frac{1}{2}}$ given by DFT is shifted to slightly larger values of D . Nevertheless, both theories agree almost precisely that $D^* \approx L$, meaning that grooves of square cross-sections become half filled with liquid at the pressure of the condensation of the capillary slits and macroscopic grooves.

The previous results revealing the importance of the competition between the two effective interactions suggest that there exists a close analogy between condensation in capillary grooves and in slit pores formed by a pair of plates with competing interactions. Within the latter model one considers a strongly attractive wall favouring the liquid phase and a wall favouring the gas phase, a

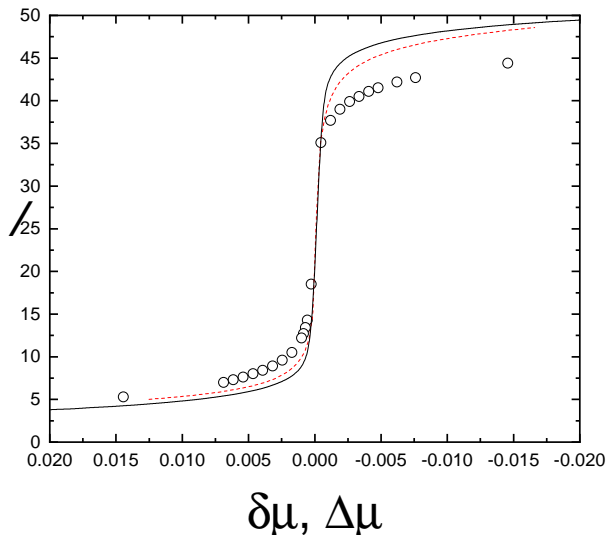


FIG. 6: Comparison of the location of the meniscus height $\ell(\delta\mu)$, where $\delta\mu = \mu_{cc} - \mu$, in a capillary groove of depth $D = 50\sigma$ and width $L = 20\sigma$ as obtained from microscopic DFT (symbols) and the full slab model using Eq. (27) (red dashed line). The black solid line shows the width of a wetting layer in a slit pore of width D formed by two competing walls with external potentials given by Eqs. (23) and (24), as a function of $\Delta\mu = \mu_{\text{sat}} - \mu$. Note that the abscissa is oriented such that μ increases from left to right.

distance D apart. Such a system may adopt three stable configurations [25, 26]: a low-density state, when the slit is filled with capillary gas, a high-density state, when the slit is filled with capillary liquid and a delocalized state, when the slit is partially filled with liquid and partially filled with gas. From a mesoscopic viewpoint, the three states can be characterised by a liquid-gas interface which is either localized near one of the walls or delocalized near a midpoint of the slit. In a bulk two-phase coexistence, $\mu = \mu_{\text{sat}}$, a transition corresponding to the depinning of the interface from either of the walls to the delocalized state may occur [25, 26], the nature of which depends on the nature of the pertinent wetting (or drying) transition. For the walls exhibiting first order transition, the localized-delocalized transition occurs at finite-size shifted wetting temperature $T^*(D)$, such that $T_w < T^* < T_{sc}$ where T_w is the wetting temperature and T_{sc} is the prewetting critical temperature [27]. Above T_{sc} , as is considered here, only the delocalized state is stable.

We now wish to map quantitatively the process of condensation in a groove of depth D and width L on the one in slit of width D formed of competing walls. Above T_{sc} the latter corresponds to a continuous shift in the location of the liquid-gas interface from the vicinity of the wetting wall to the drying one, as the chemical potential is varied around μ_{sat} . At the given μ , the location of the interface $0 < \ell < D$ is determined by a balance of the effective and oppositely directed forces, induced

by the long-range potentials of the walls. These potentials, $V^{(w)}(z)$ and $V^{(d)}(z)$, are set such that the excess grand potential per unit area for the slit model has the same structure as the one for our groove model given by Eq. (17):

$$\Omega^{\text{slit}} = \Delta\mu\Delta\rho\ell + \frac{3A_w}{8\ell^3} + \frac{A_d}{(D-\ell)^2}. \quad (21)$$

except that the shift $\delta\mu = \mu_{cc} - \mu$ is replaced by $\Delta\mu = \mu_{\text{sat}} - \mu$. Here, $A_w \equiv \pi\varepsilon_w^{(w)}\rho_w\sigma^6\Delta\rho/3$ and $A_d \equiv \pi\varepsilon_w^{(d)}\rho_w\sigma^6\Delta\rho/3$, with the parameters $\varepsilon_w^{(w)}$ and $\varepsilon_w^{(d)}$ to be determined. Thus, while the first term on the rhs of Eq. (21) measures the free energy penalty due to a departure from the two phase equilibrium, the last two terms are the binding potentials exerted by each wall. These are given by [24]

$$W_\pi = -\Delta\rho \int_\ell^\infty V_\pi(z)dz \quad (22)$$

where V_π is the corresponding wall potential [29]. From Eq. (21) it follows that the *attractive* potential of the wetting wall is

$$V^{(w)}(z) = -\frac{\varepsilon_w^{(w)}\rho_w\sigma^6}{z^4}, \quad (23)$$

with $\varepsilon_w^{(w)} = 3\pi L\varepsilon_w/8$ and the (long range) *repulsive* potential of the drying wall is

$$V^{(d)}(z) = \varepsilon_w^{(d)}\rho_w\sigma^3 \left(\frac{\sigma}{D-z}\right)^3 \quad (24)$$

with $\varepsilon_w^{(d)} = \varepsilon_w$.

In Fig. 6 we display the DFT results of the meniscus growth in a groove of depth $D = 50\sigma$ and width $L = 20\sigma$ as a function of $\delta\mu = \mu_{cc} - \mu$ and compare with the growth of the wetting layer in a slit pore with competing walls as a function of $\Delta\mu = \mu_{\text{sat}} - \mu$. The external long-ranged potentials of the slit walls given by Eqs. (23) and (24) that largely determine the adsorption behaviour in the slit are complemented with the rapidly decaying $\sim z^{-9}$ repulsive contributions that are kept the same as in Eq. (10) for both walls. We observe a reasonably good agreement showing a close link between the two processes especially for $\delta\mu > 0$; for large values of ℓ ($\delta\mu < 0$) the deviation is slightly larger, which indicates that our slab model approximation becomes less accurate when the meniscus reaches top of the groove; this conclusion is indeed supported by inspection of the density profiles shown in Fig. 3.

It should be emphasized that the simple structure of Eqs. (16) and (17) follows from the analysis of the slab model (15) near μ_{cc} where the growth of the meniscus is most dramatic. Further away from μ_{cc} , higher order terms neglected in (17) may also become important. In this case, the last term in Eq. (15) can be expressed as a

single integral

$$\begin{aligned} \Delta\rho \int_{\tilde{\ell}}^D dz \int_{\ell_\pi}^{L-\ell_\pi} dx V(x, z) &\approx \\ \approx 2\alpha_6 \Delta\rho \int_{\tilde{\ell}}^D dz &[\Psi(L - \ell_\pi, z) - \Psi(\ell_\pi, z) \\ + \Psi(L - \ell_\pi, D - \tilde{\ell}) - \Psi(\ell_\pi, D - z) &+ \frac{L - 2\ell_\pi}{z^3}] \end{aligned} \quad (25)$$

where we only considered the attractive portion of $V(x, z)$ and introduced

$$\Psi(x, z) = \int \psi_6(x, z) dx = \frac{(2x^2 - z^2)\sqrt{x^2 + z^2}}{2x^2 z^3} - \frac{x}{z^3}. \quad (26)$$

The mean height of the meniscus $\ell(\mu)$ is given by minimization of (15), $\left. \frac{d\omega^{ex}}{d\ell} \right|_{\tilde{\ell}=\ell} = 0$, so that the integral in (25) does not need to be evaluated and we obtain immediately

$$\begin{aligned} \mu = \mu_{\text{sat}} - \frac{2\gamma}{\Delta\rho(L - 2\ell_\pi)} & \\ + \frac{2\pi\varepsilon_w\rho_w\sigma^6}{L - 2\ell_\pi} [\Psi(L - \ell_\pi, \ell) - \Psi(\ell_\pi, \ell) & \\ + \Psi(L - \ell_\pi, D - \ell) - \Psi(\ell_\pi, D - \ell) + \frac{L - 2\ell_\pi}{\ell^3}] &. \end{aligned} \quad (27)$$

Associating ℓ_π with the width of a wetting layer on an infinity planar wall we can write [24]

$$\ell_\pi = \left(\frac{2\pi\varepsilon_w\rho_w\sigma^6}{3\Delta\mu} \right)^{\frac{1}{3}} \quad (28)$$

and substituting for the values of the microscopic and thermodynamic parameters as used in our DFT, the location of the meniscus $\ell(\delta\mu)$ can be obtained from Eq. (27) numerically. The resulting dependence is shown in Fig. 6 and we observe that the agreement with DFT is better than for the slit with asymmetric walls, as expected, but the improvement is not dramatic. This implies that our slab model is limited mainly by the approximation of the meniscus shape while neglecting the higher order terms in (17) is less significant.

IV. CONCLUSION

In this work we studied condensation in capillary grooves of depth D and width L formed of completely wet walls interacting with a confined fluid via long-range (dispersion) forces. As has been shown previously, condensation in macroscopically deep grooves, $D \rightarrow \infty$, is a critical process, such that an amount of adsorbed liquid, which can be characterized by a meniscus height ℓ , unbinds continuously from the groove bottom and eventually diverges according to $\ell \sim \delta\mu^{-1/4}$, as $\delta\mu = \mu_{cc} - \mu$

tends to zero, in some analogy to complete wetting phase transition on a planar wall. For D finite, the transition becomes rounded but still experiences the same power-law behaviour for small (positive) $\delta\mu$ as for infinitely deep grooves. However, this behaviour eventually breaks down in a very close neighborhood of μ_{cc} , characterized by the value $\bar{\delta}\mu$ which decays as D^{-3} with the groove depth. For $\delta\mu$ negative, or indeed for $\mu > \mu_{cc} + \bar{\delta}\mu$, the character of the condensation crosses over to the second regime where $\ell \sim D - |\delta\mu|^{-1/3}$. The behaviour of the meniscus growth can be explained using a simple slab model from which it follows that the meniscus is effectively the subject of two competing repulsive forces that act from the groove bottom and groove top, as a result of the presence of long-range intermolecular forces. The trade-off between them has a number of further consequences. In particular, right at μ_{cc} the two repulsions are balanced out and the meniscus is located at a height ℓ^* which scales as $(D^3L)^{1/4}$; note that the asymmetry in the range of the effective repulsions implies that the relative filling of grooves at $\mu = \mu_{cc}$ decays with the aspect ratio D/L as $\ell^*/D \sim (D/L)^{-1/4}$. Furthermore, we showed that the chemical potential $\mu_{\frac{1}{2}}$ at which grooves are half-filled with liquid ($\ell(\mu_{\frac{1}{2}}) = D/2$) exhibits non-monotonic dependence on D , such that $\mu_{\frac{1}{2}} = \mu_{cc}$ for $D \rightarrow \infty$ and $D \approx L$, and drops rapidly well below μ_{cc} for $D < L$. Finally, we made an explicit connection between condensation in capillary grooves and condensation in infinite slits made of asymmetric walls in a delocalized state. One of the walls interacts with the fluid via retarded dispersion forces at long distances with the potential strength depending on L , while the other wall, placed a distance D apart, interacts with the fluid with a non-retarded dispersion potential but repulsively. It should be noted that the model of the asymmetric slit where the density profile varies only in the direction perpendicular to the walls, is computationally much more tractable than that of the capillary groove where the density profiles varies in two dimensions.

These predictions may have some interesting applications in modern technologies. With advanced techniques in nano-lithography that enable the modification of the shape of solid surfaces on molecular scales, the results suggest a simple mechanism of how to control an amount of adsorbed liquid on the microscopic level. Consider a solid wall into which a network of capillary grooves is carved. From the slab model it follows that a small change in the chemical potential from $\mu = \mu_{cc} - \delta\mu$ to $\mu = \mu_{cc} + \delta\mu$, with $\delta\mu > 0$, induces the growth of the meniscus height by the value $\delta\ell = D - (A/\delta\mu)^{1/3} - (AL/\delta\mu)^{1/4}$. This tells us that the adsorption responses sensitively by tuning the chemical potential, i.e. the vapour pressure, around μ_{cc} (p_{cc}), and scales linearly with the groove depth D . Thus, even a very small change in external conditions can be used to control the amount of the liquid adsorbed in a micro-porous medium which can still be maintained (macroscopically) dry on its top and may thus be used as a storage of the adsorbate.

We conclude with some remarks regarding phenomena that have been omitted in this work and its possible extensions. Firstly, capillary grooves may exhibit a pre-filling characterised by a jump in the meniscus height for temperatures near the wetting temperature [13]; this is closely related to pre-wetting but in contrast to the latter is one-dimensional in nature and thus becomes necessarily rounded if thermal fluctuations are considered. The temperature considered here was deliberately chosen high enough to be beyond this temperature range, so that the condensation is always continuous even on a mean-field level. Secondly, both treatments used in this work, the slab model and DFT, neglect the effect of interfacial fluctuations, such as those in the meniscus height along the groove. However, the only effect of the fluctuations is that the condensation asymptotic regime $\ell \sim \delta\mu^{-1/4}$ would eventually crossover to $\ell \sim \delta\mu^{-1/3}$ in a very close neighborhood of μ_{cc} [18]; this effect is utterly irrelevant for finite D though since this region which is of the order of $\mathcal{O}(L^{-11})$ overlaps with the crossover region of the characteristic width $\bar{\delta}\mu$ as given by Eq. (18), anyway. Possible extensions of the current work include a study of a model of heterogeneous grooves where the side walls are of a different material than the bottom wall, extending Ref. [28] to finite values of D . Compared to the present study, this would not affect the nature of the effective repulsion from the groove top which would still contribute as $\propto (D - \ell)^{-2}$ to the grand potential but the repulsion from the groove bottom would now be $\propto \ell^{-2}$, i.e. the forces are of the same range. One of the consequences would be that ℓ^* is now independent of L and scales linearly with D , with the proportionality constant given by the difference in the wall potential strengths. Also, it would be interesting to inspect the impact of the finite-size effects at different wall geometries, such as linear wedges or cylinders. Finally, the extension of the current model to a periodic system of parallel grooves would allow to investigate the nature of the liquid-gas interface as $\mu \rightarrow \mu_{\text{sat}}$ and the effect of its undulation to the process of complete wetting. Some of these problems will be subject of our future work.

V. APPENDIX A. ESTIMATION OF $\bar{\delta}\mu$

For $\mu \approx \mu_{cc}$, the magnitudes of the effective repulsive terms in Eq. (16) are comparable while for a sufficient deviation from μ_{cc} one of the two terms in the bracket becomes dominant; in this Appendix we estimate such a minimal deviation $\bar{\delta}\mu$ for each case.

To this end, we define the new length-scale $x \equiv (a/|\bar{\delta}\mu|)^{1/3}$ and express Eq. (16) in the form

$$\frac{1}{x^3} \approx \frac{L}{\ell^4} - \frac{1}{(D - \ell)^3} \quad (29)$$

where we ignored unimportant multiplicative constants. We now consider the cases $\mu < \mu_{cc}$ and $\mu > \mu_{cc}$ separately.

A. $\mu < \mu_{cc}$

In this case we are looking for a condition under which

$$\frac{L}{\ell^4} \gg \frac{1}{(D - \ell)^3} \quad (30)$$

implying

$$D \gg x + \ell \quad (31)$$

and

$$x \approx \left(\frac{\ell^4}{L} \right)^{\frac{1}{3}}. \quad (32)$$

By combining Eqs. (31) and (32) it follows that

$$D \gg \ell \left[1 + \left(\frac{\ell}{L} \right)^{\frac{1}{3}} \right]. \quad (33)$$

We may now distinguish between two regimes, depending on the relative values of ℓ and L . If $\ell \gg L$, then the last term in Eq. (33) dominates compared to unity and thus $D \gg (\ell^4/L)^{\frac{1}{3}}$. Upon using Eq. (32) and substituting for x this implies that the relation in Eq. (30) is obeyed provided $\bar{\delta}\mu \gg a/D^3$.

For $\ell \ll L$, the last term in Eq. (33) is negligible compared to unity and the condition (30) requires that $D \gg \ell$ leading to $\bar{\delta}\mu \gg aL/D^4$. This differs from the previous result only if L appreciably deviates from D . Clearly, the possibility $L \gg D$ is excluded since the groove geometry would not allow for a meniscus formation. On the other hand, $L \ll D$ would mean that the condition $\bar{\delta}\mu \gg a/D^3$ is more restrictive than $\bar{\delta}\mu \gg aL/D^4$. This is however straightforward to show that within the former regime $x \gg \ell \gg L$ whilst in the latter case we have $x \ll \ell \ll L$ and recalling that $\bar{\delta}\mu \propto 1/x$ these results contradict the previous statement.

Finally, the intermediate case $\ell \sim L$ can only be realized if $L \ll D$ in order the condition (30) to be fulfilled. Then (31) reduces to $D \gg x$ leading again to $\bar{\delta}\mu \gg a/D^3$.

B. $\mu > \mu_{cc}$

Above μ_{cc} the situation is just opposite, i.e. we require

$$\frac{L}{\ell^4} \ll \frac{1}{(D - \ell)^3}, \quad (34)$$

from which (together with Eq. (29)) it follows that

$$D \approx x + \ell \quad (35)$$

and

$$D \ll \ell \left[1 + \left(\frac{\ell}{L} \right)^{\frac{1}{3}} \right], \quad (36)$$

Now, since $\ell < D$, we can write

$$D \ll \left(\frac{\ell^4}{L} \right)^{\frac{1}{3}}, \quad (37)$$

which on using of (35) leads after some rearrangements to

$$D \left[1 - \left(\frac{L}{D} \right)^{\frac{1}{4}} \right] \gg x. \quad (38)$$

Since $x > 0$, the last condition is satisfied only if $D \gg x$ reproducing (18) again.

Acknowledgments

The support from the Czech Science Foundation, project 17-25100S, is acknowledged.

-
- [1] J. S. Rowlinson and B. Widom, *Molecular Theory of Capillarity*, Oxford, Clarendon, (1982).
- [2] R. Evans, J. Phys.: Cond. Matter. **2**, 8989 (1990).
- [3] B. V. Derjaguin, Zh. Fiz. Khim. **137**, 14 (1940).
- [4] R. Evans and U. Marini Bettolo Marconi, Chem. Phys. Lett. **114**, 415 (1985).
- [5] R. Evans, U. Marini Bettolo Marconi, and P. Tarazona, J. Chem. Soc. Faraday Trans. **2**, 1763 (1986).
- [6] R. Evans, Adv. Phys. **28**, 143 (1979).
- [7] G. A. Darbellay and J. M. Yeomans, J. Phys. A **25**, 4275 (1992).
- [8] C. Rascón, A. O. Parry, N. B. Wilding, and R. Evans, Phys. Rev. Lett. **98**, 226101 (2007).
- [9] M. Tasinkevych and S. Dietrich, Eur. Phys. J. **E23**, 117 (2007).
- [10] L. Bruschi and G. Mistura, J. Low Temp. Phys. **157**, 206 (2009).
- [11] T. Hofmann, M. Tasinkevych, A. Checco, E. Dobisz, S. Dietrich, and B. M. Ocko, Phys. Rev. Lett. **104**, 106102 (2010).
- [12] H. Boelen, A. O. Parry, E. Diaz-Herrera and M. Schoen, Eur. Phys. J. E **25**, 103 (2008).
- [13] A. Malijevský, J. Chem. Phys. **137**, 214704 (2012).
- [14] C. Rascón, A. O. Parry, R. Nürnberg, A. Pozzato, M. Tormen, L. Bruschi, and G. Mistura, J. Phys.: Condens. Matter **25**, 192101 (2013).
- [15] P. Yatsyshin, N. Savva, and S. Kalliadasis, Phys. Rev. E **87**, 020402 (2013).
- [16] A. Malijevský, J. Phys.: Cond. Matter **25**, 445006 (2013).
- [17] G. Mistura, A. Pozzato, G. Greci, L. Bruschi, and M. Tormen, Nat. Commun. **4**, 2966 (2013).
- [18] A. Malijevský and A. O. Parry, J. Phys: Condens. Matter **26**, 355003 (2014).
- [19] D. Schneider, R. Valiullin, and P.A. Monsosn, Langmuir **30**, 1290 (2014).
- [20] C. Fan, D.D. Do, and D. Nicholson, Mol. Simul. **41**, 245 (2014).
- [21] L. Bruschi, G. Mistura, P.T.M. Nguyen, D.D. Do, D. Nicholson, S. J. Park, and W. Lee, Nanoscale **7**, 2587 (2015).
- [22] A. Malijevský and A. Parry, Phys. Rev. Lett., in press.
- [23] Y. Rosenfeld, Phys. Rev. Lett. **63**, 980 (1989).
- [24] S. Dietrich, in *Phase Transitions and Critical Phenomena*, edited by C. Domb and J. L. Lebowitz (Academic, New York, 1988), Vol. 12.
- [25] A. O. Parry and R. Evans, Phys. Rev. Lett. **64**, 439 (1990).
- [26] A. O. Parry and R. Evans, Physica A **181**, 250 (1992).
- [27] A. Malijevský, Cond. Matt. Phys. **19**, 13604 (2016).
- [28] A. O. Parry, A. Malijevský and C. Rascón, Phys. Rev. Lett. **113**, 146101 (2014).
- [29] We recall that the fluid-fluid potential is truncated, i.e. short-ranged, and thus does not contribute to the binding potential.